



3E analysis and multi-objective optimization of a trans-critical ejector-assisted CO₂ refrigeration cycle combined with thermo-electric generator

Shoaib Khanmohammadi¹ · Mohammad Reza Sharifinasab¹

Received: 25 September 2023 / Accepted: 27 January 2024 / Published online: 18 March 2024
© Akadémiai Kiadó, Budapest, Hungary 2024

Abstract

Conserving energy is an important factor in industry which could lead to reduce the operating costs of the system. Improving energy efficiency is a serious concern to many researchers and numerous studies have been conducted on this goal. A valuable method to locate the inefficient system components is the conventional exergy analysis. Furthermore, to estimate the cost efficiency of a thermodynamic system, exergo-economic analysis is indispensable. This study evaluates the ejector trans-critical CO₂ refrigeration cycle from exergo-economic viewpoint. The thermodynamic system was modeled using Engineering Equation Solver (EES) software. In order to utilize the waste heat of the gas cooler, a thermo-electric generator is introduced. Energy, exergy, and exergo-economic (3E) analysis has been performed. A parametric study was conducted of gas cooler pressure, low-pressure compressor outlet pressure, and evaporator pressure. Multi-criteria optimization has been conducted to optimize COP and refrigeration cost rate using NSGA-II (non-dominated sorting genetic algorithm). The results showed the system could provide a COP of 1.593 for the base case of the cycle operation. The high-priority components to improve were expansion valve, thermo-electric generator, and low-pressure compressor which had the highest exergy destruction ratio as 0.211, 0.180, and 0.158 respectively. The refrigeration cost rate was 2.898 \$ h⁻¹ for the base case of the system. Optimization results showed that the exergy efficiency and the exergy destruction ratio of the optimum design point are 0.284 and 0.574.

Keywords Trans-critical CO₂ refrigeration system · Ejector · Exergo-economic analysis · Multi-objective optimization

List of Symbols

e	Specific exergy (kJ kg ⁻¹)
\dot{E}	Exergy rate (kW)
h	Specific enthalpy (kJ kg ⁻¹)
\dot{m}	Mass flow rate (kg s ⁻¹)
P	Pressure (kPa)
P	Power (kW)
\dot{W}	Work (kW)
\dot{Q}	Heat transfer (kW)
s	Specific entropy (kJ kg ⁻¹ K ⁻¹)
T	Temperature (K) – (°C)
v	Velocity (m s ⁻¹)
x	Quality
\dot{C}	Cost rate (\$ h ⁻¹)
c	Specific exergy cost (\$ GJ ⁻¹)

Z	Investment cost of component (\$)
\dot{Z}	Investment cost rate of component (\$ h ⁻¹)
α	Seebeck coefficient (V K ⁻¹)
σ	Electrical conductivity (S m ⁻¹)
λ	Thermal conductivity (W m ⁻¹ K ⁻¹)
ω	Entrainment ratio of ejector
η	Efficiency
δ	Exergy destruction ratio

Superscripts

T	Thermal
M	Mechanical

Subscripts

do	Diffuser outlet
D	Destruction
hpc	High-pressure compressor
lpc	Low-pressure compressor
ex	Exergy
F	Fuel
P	Product

✉ Shoaib Khanmohammadi
sh.khanmohammadi@kut.ac.ir

¹ Department of Mechanical Engineering, Kermanshah University of Technology, Kermanshah, Iran

L	Loss
is	Isentropic
n	Nozzle
d	Diffuser
m	Mixing chamber
high	High-pressure stage
low	Low-pressure stage
in	Inlet
out	Outlet
teg	Thermo-electric generator
0	Reference parameter

Introduction

Using CO₂ as a refrigerant has the benefit of low global warming potential (GWP). Another advantage of CO₂ refrigerant is its ozone depletion potential (ODP) which is zero and it has no negative impact on the ozone layer. Striking features of CO₂ refrigerant such as non-flammability, inexpensiveness, and availability increases its practical application in industry [1, 2]. Hydrofluorocarbons such as R134a are detrimental to environment due to their high GWP index in contrast to CO₂ refrigerant [3]. To increase the performance of refrigeration systems, numerous strategies such as applying an expander [4, 5], vortex tube [6], mechanical subcooling [7, 8], and cascade CO₂ – NH₃ refrigeration cycle [9, 10] has been implemented. Due to distinguishing features such as simple geometry, and lack of intricate parts, the ejector refrigeration systems received the attention of designers [11, 12]. Ejector could assist the compressor and decreases compressor work accordingly [13]. The ejector increases the inlet pressure of the following compressor, consequently, it reduces the compressor input work [14]. The ejector could improve the flow rate, evaporator heat exchange, and the exergy efficiency [15].

Wang et al. [16] studied a trans-critical CO₂ ejector heat pump. Their study evaluated the CO₂ heat pump system which includes an ejector device. In their study, the system was investigated from exergy and sensitivity analyses viewpoints. According to their results, the COP of the cycle with ejector and internal heat exchanger increased by 7.38% at 15 °C ambient temperature and the pressure ratio reduced to 2.66. Their results showed the exergy destruction rate of throttling valve was decreased when ejector was applied to the heat pump system.

Casi et al. [17] evaluated the performance of a CO₂ refrigeration plant using a thermo-electric subcooler experimentally. Their study utilizes internal heat exchanger and thermo-electric subcooler together. The experiments have been conducted at different ambient temperature and ambient relative humidity. The optimum pressure of the gas cooler was 71 bar and optimum voltage of thermo-electric

devices was 2 V. The experiments reports stated that 22.4% increase in COP was achieved at 35 °C ambient temperature and 75% relative humidity.

Eskandari and Cheraghi [13] investigated a refrigeration cycle with two ejectors. The ejector was modeled using a one-dimensional method. Their proposed new system includes two ejectors and two separators. According to the results, the power consumption for compressor decreased and as a result the gas cooler waste heat decreased. The optimum gas cooler working pressure was 10,000 kPa. The results demonstrated that the exergy destruction rates for each of the components in the proposed cycle decreased in comparison to conventional ejector cycle.

Liu et al. [12] performed a study on a system using two evaporators and two ejectors for supermarkets application. Their cycle utilizes a flash tank. The first ejector increases the main flow of the other one and consequently lift the inlet pressure of the compressor. According to the results, up to 19.1% reduction in pressure ratio was obtained, and COP could improve to 27.1% in comparison to the conventional cycle which includes two evaporators. The optimum pressure of gas cooler for the proposed cycle was around 8.15 MPa.

Santini et al. [18] conducted an experimental and theoretical investigation on trans-critical CO₂ cycle. The experimental system utilizes one compressor and it doesn't use ejectors. According to their reports, there was a considerable exergy destruction in high pressure expansion valve which was 27.19% of total irreversibility in the experimental operating cycle. In order to overcome this drawback, the expansion valve was replaced by an ejector in a theoretical thermodynamic model. It was obtained that COP is highly dependent on the entrainment ratio and higher COP could be achieved as entrainment ratio rises higher than 0.6. The ejector assisted the cycle in decreasing the temperature of compressor outlet and also it decreased the power consumption of compressor.

Aranguren et al. [19] conducted an experimental test of trans-critical single stage CO₂ refrigeration plant including a thermo-electric subcooler. The tests are done on experimental system under relative humidity of 55%. The thermo-electric was placed at the outflow of the gas cooler and they were in series configuration. The capacity of cooling was about 280 W. The applied thermo-electric had four copper blocks. The results demonstrated the optimum COP was 1.15 for the overall system. At this optimal working condition there was a 15.3% rise in cooling capacity compared to the cycle without thermo-electric subcooler.

In this paper, the ejector two-stage trans critical refrigeration cycle is analyzed from energy, exergy, and exergo-economic viewpoints. The cycle was modeled by Engineering Equation Solver (EES). A parametric study has been performed to evaluate the effects of gas cooler pressure,

evaporator pressure (saturation temperature), and low-pressure compressor discharge pressure on the COP. Energy, exergy, and exergo-economic analyses were conducted to determine the inefficiencies in cycle operation. In addition, a multi-objective optimization using genetic algorithm, has been conducted to achieve a balance between the coefficient of performance and refrigeration cost rate. A thermo-electric generator (TEG) was applied for converting waste heat to electricity. Studying components under different operating conditions such as different operating pressures is essential to enhance the efficiency of the refrigeration cycle [20]. Applying a thermo-electric generator is a method to utilize waste heat from an industrial component, it also has no moving parts and has a low maintenance cost [21].

System properties and assumptions

The components and property diagram of the introduced cycle are depicted in Figs. 1 and 2, respectively. The CO₂ refrigerant first comes from the intercooler in the saturated vapor phase (state 1) then the high-pressure compressor is conducting a pressure raise and the refrigerant reaches a high pressure (state 2). The gas then transfers heat to the cooling water (state 3) and then is used for preheating the evaporator output flow, through the heat exchanger (state 4). Then it enters the primary nozzle and is mixed in the mixing chamber with the outflow of the low-pressure compressor, and finally passes the diffuser to be pressurized (state 5). In the intercooler, input flows which are ejector output (state 5) and medium pressure expansion valve output (state 11), exchange heat. Then saturated vapor and

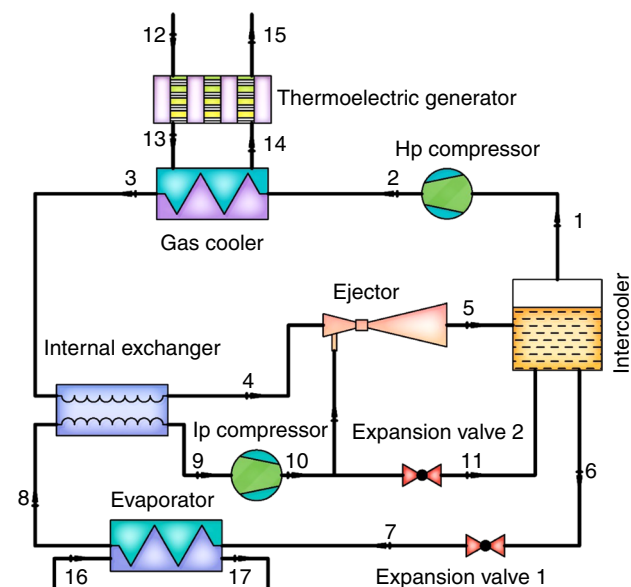


Fig. 1 Schematic diagram of the refrigeration cycle

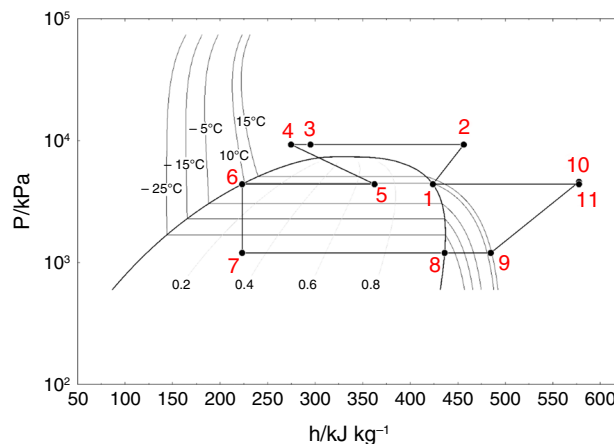


Fig. 2 Phase diagram of the studied refrigeration cycle

saturated liquid flow and enter the compressor and the expansion valve, respectively (state 1 and state 6).

After throttling by low-pressure expansion valve (state 7), the refrigerant enters the evaporator and performs cooling and exchanging heat with the air stream. After the evaporator (state 8), refrigerant passes through the internal heat exchanger and enters the compressor (state 9). Then one part of the refrigerant enters the ejector and the other part is throttled through the medium-pressure expansion valve and enters the intercooler. Two separate water streams are used to transfer the excess heat from the gas cooler. For simplicity of simulation some assumptions are considered as follows [20]:

- The adiabatic non-isentropic compression processes occur in the refrigeration cycle.
- Fluid mixing in the mixing chamber takes place at constant pressure.
- The pressure and temperature of the atmospheric state are $P_0 = 101.325\text{kPa}$ and $T_0 = 25^\circ\text{C}$ respectively.
- Pressure drops and heat loss of internal heat exchanger, evaporator, gas cooler, pipes, and intercooler are ignored.
- The temperature of the inlet water and outlet water of the gas cooler and inlet air and outlet air of the evaporator and inlet water and outlet of the thermo-electric generator cold side (state 12) remain fixed during the cycle.
- The kinetic energy of the inlet flow of the ejector is ignored.
- The state points of flowing air through the evaporator (states 16 and 17) are fixed, i.e., refrigeration capacity is constant [20].
- The inlet and output states of internal heat exchanger, are remained fixed (Fig. 3).

Energy and exergy analysis

Energy model

According to previous assumptions, the energy model was obtained using mass and energy conservations.

For compressors:

$$W_{\text{ipc}} = \dot{m}_{\text{ipc}}(h_{10} - h_9) \quad (1)$$

$$W_{\text{hpc}} = \dot{m}_{\text{hpc}}(h_2 - h_1) \quad (2)$$

$$\eta_{\text{ipc}} = \frac{h_{10,\text{is}} - h_9}{h_{10} - h_9} \quad (3)$$

$$\eta_{\text{hpc}} = \frac{h_{2,\text{is}} - h_1}{h_2 - h_1} \quad (4)$$

where W_{ipc} , W_{hpc} , and h_{is} are the low-pressure compressor input power, high-pressure compressor input power, and isentropic enthalpy of the compressors outlet, respectively. According to Ref. [22], the compressors adiabatic efficiencies are:

$$\eta_{\text{ipc}} = 0.815 + 0.022 \left(\frac{P_{10}}{P_9} \right) - 0.0041 \left(\frac{P_{10}}{P_9} \right)^2 + 0.0001 \left(\frac{P_{10}}{P_9} \right)^3 \quad (5)$$

$$\eta_{\text{hpc}} = 0.815 + 0.022 \left(\frac{P_2}{P_1} \right) - 0.0041 \left(\frac{P_2}{P_1} \right)^2 + 0.0001 \left(\frac{P_2}{P_1} \right)^3 \quad (6)$$

where η is the adiabatic efficiency and could be calculated using the inlet and outlet pressure of each compressor. For evaporator refrigeration capacity:

$$\dot{Q}_{\text{evaporator}} = \dot{m}_{\text{low}}(h_8 - h_7) \quad (7)$$

where $\dot{Q}_{\text{evaporator}}$ is the heat transfer rate in evaporator. The outflow of the internal exchanger enters the ejector primary inlet and the outflow of the compressor enters the ejector's secondary inlet. Finally, after mixing process, the mixture is expanded and flows toward the intercooler. The governing equations for ejector are as follows [23]. Using the first law of thermodynamics, the velocity out of the nozzle can be derived as:

$$v_p = \sqrt{2\eta_n(h_{n,\text{in}} - h_{n,\text{out},\text{is}})} \times 1000 \quad (8)$$

where $h_{n,\text{in}}$ is the specific enthalpy of the ejector's primary inlet and $h_{n,\text{out},\text{is}}$ is the exit isentropic specific enthalpy in the nozzle with constant pressure which is equal to low-pressure compressor discharge. Considering momentum

conservation, velocity of the mixture in mixing chamber v_m can be derived as:

$$v_m = \frac{v_p}{1 + \omega} \sqrt{\eta_m} \quad (9)$$

where ω is the entrainment ratio of the ejector. Applying the first law of thermodynamics, the specific enthalpy of mixed refrigerant h_m is calculated as:

$$h_m = \frac{h_{n,\text{in}} + \omega h_{\text{sec},\text{in}}}{1 + \omega} - \frac{v_m^2}{2 \times 1000} \quad (10)$$

where $h_{\text{sec},\text{in}}$ is the specific enthalpy of the secondary inlet.

By applying the diffuser efficiency, the enthalpy at the ejector outlet could be derived as:

$$h_d = h_m + \frac{h_{d,\text{out},\text{is}} - h_m}{\eta_d} \quad (11)$$

where $h_{d,\text{out},\text{is}}$ is the diffuser exit isentropic specific enthalpy.

Using energy conservation, the velocity at the outlet of the ejector is derived as:

$$v_d = \sqrt{v_m^2 - 2(h_d - h_m) \times 1000} \quad (12)$$

The entrainment ratio is obtained by an iteration based on Fig. 4. Applying a mass balance through the two-phase ejector, the quality x_{do} is derived as a function of entrainment ratio i.e.:

$$x_{\text{do}} = \frac{1}{1 + \omega} \quad (13)$$

A tolerance of 0.01 is used for convergence. Applying the first law of thermodynamics to ejector:

$$h_4 + \omega h_{10} = (1 + \omega) \cdot \left(h_5 + \frac{v_d^2}{2000} \right) \quad (14)$$

The assumptions for the iterative process to calculate entrainment ratio are pressures and temperatures of primary and secondary inlets, the outlet pressure of ejectors, and mixing chamber, diffuser, and nozzle efficiencies. These parameters are used to calculate the velocities and enthalpies of the ejector different parts. Finally, the calculated entrainment ratio is used to calculate the mass flow rate of high-pressure stage of the cycle (Table 1).

For thermo-electric generators according to Ref. [24] the equations are as follows:

$$Q_{\text{h,TEG}} = \dot{m}_{\text{water}}(h_{14} - h_{13}) \quad (15)$$

where $Q_{\text{h,TEG}}$ is the heat received from gas cooler water.

$$P_{\text{TEG}} = Q_{\text{h,TEG}} \times \eta_{\text{TEG}} \quad (16)$$

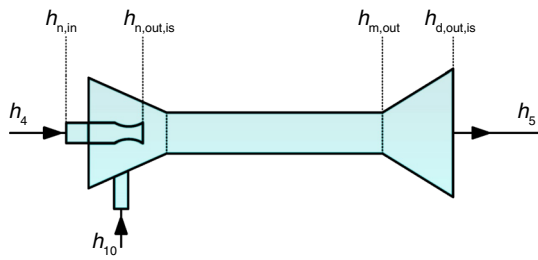


Fig. 3 Schematic diagram of two-phase ejector

where P_{TEG} is the generated power of the thermo-electric generator.

The thermo-electric generator efficiency (η_{TEG}) is defined as a function of Carnot efficiency (η_{Carnot}), working temperatures, and material properties.

$$\eta_{TEG} = \eta_{Carnot} \times \frac{\sqrt{1 + ZT_{average}} - 1}{\sqrt{1 + ZT_{average}} + \frac{T_c}{T_h}} \tag{17}$$

$$\eta_{Carnot} = \frac{T_h - T_c}{T_h} \tag{18}$$

$ZT_{average}$ is the non-dimensional figure of merit of the semiconductor and is defined as:

$$ZT_{average} = \frac{\alpha^2 \times \sigma}{\lambda} \times \frac{(T_h + T_c)}{2} \tag{19}$$

where T_h , T_c , and $T_{average}$ are the average temperature of hot side, the average temperature of the cold side, and the average operating temperature of the thermo-electric generator, respectively. The properties of thermo-electric are listed in Table 2.

For calculating the high-stage refrigerant mass flow rate, the following mass balance at low-pressure compressor node is written:

$$\dot{m}_{low} = \omega \dot{m}_{high} + \dot{m}_{11} \tag{20}$$

Which \dot{m}_{low} could be calculated using energy balance across the evaporator. The COP of the system was calculated as follows:

$$COP = \frac{Q_e}{W_{lpc} + W_{hpc} - P_{TEG}} \tag{21}$$

Exergy analysis

The ability of a system to produce work during a set of processes to reach equilibrium with the environment is defined as exergy. Conventional exergy analysis (CEA) is a usual method for measuring irreversibility of components [25]. The CEA, can determine the position and size of the exergy destruction in system components [26]. The Flow exergy of each state point was calculated as [20]:

$$\dot{E}_j = \dot{m} \cdot e_j = \dot{m} \cdot [(h_j - h_0) - T_0(s_j - s_0)] \tag{22}$$

where subscript j indicates the 1–17 state points in the cycle property diagram (Fig. 2) and subscript 0 indicates the reference state point. For kth component of the system, the conventional exergy balance can be written as:

$$\dot{E}_{F,k} = \dot{E}_{P,k} + \dot{E}_{D,k} \tag{23}$$

The flow exergy of each line can be separated into thermal and mechanical exergy i.e.:

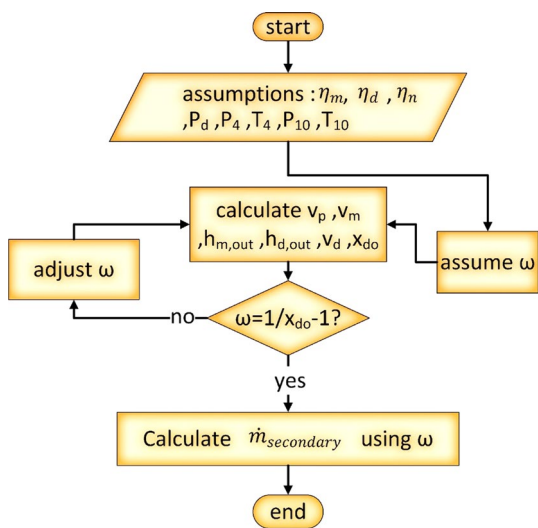


Fig. 4 Flowchart of ejector entrainment ratio calculations

Table 1 Parameters and assumptions for ejector [20]

Parameters	Value
Nozzle efficiency/ η_n	0.75
Mixing chamber efficiency/ η_m	0.9
Diffuser efficiency/ η_d	0.9

Table 2 Thermo-electric material properties [24]

Coefficient	Full name	value
α	Seebeck coefficient	$2.2 \times 10^{-4} (V K^{-1})$
σ	electrical conductivity	$1 \times 10^5 (S m^{-1})$
λ	thermal conductivity	$1.5 (W m^{-1} K^{-1})$

Table 3 Fuel and product exergy equation for each system component

Component	Fuel exergy	Product exergy	Exergy destruction
Gas cooler	$\dot{E}_F = \dot{m}_{high}(e_2 - e_3)$	$\dot{E}_P = \dot{m}_{13}(e_{14} - e_{13})$	$\dot{E}_D = \dot{m}_{high}(e_2 - e_3) - \dot{m}_{13}(e_{14} - e_{13})$
Internal heat exchanger	$\dot{E}_F = \dot{m}_{high}(e_3 - e_4)$	$\dot{E}_P = \dot{m}_{low}(e_9 - e_8)$	$\dot{E}_D = \dot{m}_{high}(e_3 - e_4) - \dot{m}_{low}(e_9 - e_8)$
Ejector	$\dot{E}_F = \dot{m}_{high}(e_4 - e_5)$	$\dot{E}_P = \omega \dot{m}_{high}(e_{10} - e_5)$	$\dot{E}_D = \dot{m}_{high}[(e_4 - e_5) - \omega(e_{10} - e_5)]$
Intercooler	$\dot{E}_F = \dot{m}_5 e_5 + \dot{m}_{11} e_{11}$	$\dot{E}_P = \dot{m}_1 e_1 + \dot{m}_6 e_6$	$\dot{E}_D = [\dot{m}_5 e_5 + \dot{m}_{11} e_{11}] - [\dot{m}_1 e_1 + \dot{m}_6 e_6]$
Expansion valve 1	$\dot{E}_F = \dot{m}_{low}(e_6^M - e_7^M + e_6^T)$	$\dot{E}_P = \dot{m}_{low} e_7^T$	$\dot{E}_D = \dot{m}_{low}(e_6^M - e_7^M + e_6^T - e_7^T)$
Evaporator	$\dot{E}_F = \dot{m}_{low}(e_7 - e_8)$	$\dot{E}_P = \dot{m}_{16}(e_{17} - e_{16})$	$\dot{E}_D = \dot{m}_{low}(e_7 - e_8) - \dot{m}_{16}(e_{17} - e_{16})$
Low-pressure compressor	$\dot{E}_F = W_{lpc}$	$\dot{E}_P = \dot{m}_{low}(e_{10} - e_9)$	$\dot{E}_D = W_{lpc} - \dot{m}_{low}(e_{10} - e_9)$
High-pressure compressor	$\dot{E}_F = W_{hpc}$	$\dot{E}_P = \dot{m}_{high}(e_2 - e_1)$	$\dot{E}_D = W_{hpc} - \dot{m}_{high}(e_2 - e_1)$
Expansion valve 2	$\dot{E}_F = (\dot{m}_{low} - \omega \dot{m}_{high}) \cdot (e_{10}^M - e_{11}^M + e_{10}^T)$	$\dot{E}_P = (\dot{m}_{low} - \omega \dot{m}_{high}) e_{11}^T$	$\dot{E}_D = (\dot{m}_{low} - \omega \dot{m}_{high}) \cdot (e_{10}^M - e_{11}^M + e_{10}^T - e_{11}^T)$
Thermo-electric generator	$\dot{E}_F = \dot{m}_{14}(e_{14} - e_{13})$	$\dot{E}_P = P_{TEG}$	$\dot{E}_D = \dot{m}_{14}(e_{14} - e_{13}) - P_{TEG}$

Table 4 Exergo-economic data [27]

Parameter	Value
System life, n	20 years
Maintenance factor, φ	1.06
Interest rate, i_r	10%
System operating hours in a year, N	7446 h

$$e = e_{jT} + e_{jM} = \left[(h_{j-h P_j, T_0}) - T_0 (s_j - s_{P_j, T_0}) \right]_{P=\text{const}} + \left[(h_{P_j, T_0} - h_0) - T_0 (s_{P_j, T_0} - s_0) \right]_{T=\text{const}} \quad (24)$$

The total exergy balance is:

$$\dot{E}_{F,\text{total}} = \dot{E}_{P,\text{total}} + \sum \dot{E}_{D,k} + \dot{E}_{L,\text{total}} \quad (25)$$

$\dot{E}_{L,\text{total}}$ is the exergy that cannot be used in the system and can be calculated using Eq. (22). In the CEA method, to assess component and overall system performance, the following parameters are defined:

$$\eta_k = \frac{\dot{E}_{P,k}}{\dot{E}_{F,k}} \quad (26)$$

$$\eta_{\text{ex}} = \frac{\dot{E}_{P,\text{total}}}{\dot{E}_{F,\text{total}}} \quad (27)$$

$$\delta_k = \frac{\dot{E}_{D,k}}{\sum \dot{E}_{D,k}} \quad (28)$$

Table 5 The investment costs of components [29–31]

Component	Equation
High-pressure compressor	$Z_{hpc} = \left(\frac{75 \dot{m}_{high}}{0.9 - \eta_{hpc}} \right) \left(\frac{P_{out}}{P_{in}} \right) \ln \left(\frac{P_{out}}{P_{in}} \right)$
Low-pressure compressor	$Z_{lpc} = \left(\frac{75 \dot{m}_{low}}{0.9 - \eta_{lpc}} \right) \left(\frac{P_{out}}{P_{in}} \right) \ln \left(\frac{P_{out}}{P_{in}} \right)$
Expansion valve 1	$Z_{ev1} = 0$
Expansion valve 2	$Z_{ev2} = 0$
Ejector	$Z_{ejector} = 0$
Intercooler	$Z_{intercooler} = 0$
Gas cooler	$Z_{\text{gas cooler}} = 2143A_{gc}^{0.514}$
Internal exchanger	$Z_{\text{int. heat exchanger}} = 2143A_{\text{int. hex}}^{0.514}$
Evaporator	$Z_{\text{evaporator}} = 16000(A_{\text{evaporator}}/100)^{0.6}$
Thermo-electric generator	$Z_{\text{teg}} = 2000P_{\text{teg}}$

$$\delta_{\text{ex}} = \frac{\sum \dot{E}_{D,k}}{\dot{E}_{F,\text{total}}} \quad (29)$$

η_k and η_{ex} are the exergy efficiency of each component and the exergy efficiency of the overall system, and δ_k and δ_{ex} are the exergy destruction ratios of each component and overall system, respectively [20] (Table 3, 4, 5 and 6).

Exergo-economic analysis

Economy factor is an indispensable part in engineering applications. In order to calculate the cost for the exergy of streams, exergo-economic analysis complements the exergy analysis [27]. Exergo-economic analysis is a

Table 6 Cost balance equation for exergo-economic analysis

Component	Cost rate balance equation	Auxiliary equation
High-pressure compressor	$\dot{C}_1 + \dot{Z}_{hpc} + \dot{C}_{w,hpc} = \dot{C}_2$	$c_w = 0.093\$/kWh[32]$
Gas cooler	$\dot{C}_2 + \dot{C}_{13} + \dot{Z}_{gc} = \dot{C}_3 + \dot{C}_{14}$	$c_2 = c_3 c_{13} = c_{14}$
Internal heat exchanger	$\dot{C}_3 + \dot{C}_8 + \dot{Z}_{ihe} = \dot{C}_4 + \dot{C}_9$	$c_3 = c_4$
Low-pressure compressor	$\dot{C}_9 + \dot{Z}_{lpc} + \dot{C}_{w,lpc} = \dot{C}_{10}$	$c_w = 0.093\$/kWh$
Ejector	$\dot{C}_4 + \left(\frac{\dot{m}_{10} - \dot{m}_{11}}{\dot{m}_{10}}\right)\dot{C}_{10} + \dot{Z}_{ejector} = \dot{C}_5$	–
Expansion valve 2	$\left(\frac{\dot{m}_{11}}{\dot{m}_{10}}\right)\dot{C}_{10} + \dot{Z}_{ev2} = \dot{C}_{11}$	–
Intercooler	$\dot{C}_5 + \dot{C}_{11} + \dot{Z}_{inc} = \dot{C}_1 + \dot{C}_6$	$c_1 = c_6$
Expansion valve 1	$\dot{C}_6 + \dot{Z}_{ev1} = \dot{C}_7$	–
Evaporator	$\dot{C}_7 + \dot{C}_{16} + \dot{Z}_{evap} = \dot{C}_8 + \dot{C}_{17}$	$c_7 = c_8, c_{16} = c_{17}, c_{12} = 0$
Thermo-electric generator	$\dot{C}_{14} + \dot{C}_{12} + \dot{Z}_{teg} = \dot{C}_{13} + \dot{C}_{15} + \dot{C}_{p,teg}$	$c_{p,teg} = c_{15}$

powerful technique for specifying cost- effectiveness of a thermodynamic system [28]. For each component, the cost balance is written as [27]:

$$\dot{Z}_k + \dot{C}_q + \sum \dot{C}_i = \sum \dot{C}_e + \dot{C}_w \tag{30}$$

where \dot{Z}_k , \dot{C}_q , \dot{C}_i , \dot{C}_e , and \dot{C}_w are the total investment, heat transfer, inlet stream, exit stream, and work cost rate for each component in the system.

The ratio of cost rate to exergy rate is defined as specific exergy cost:

$$c_j = \frac{\dot{C}_j}{\dot{E}_j} \tag{31}$$

Total investment cost rate could be calculated using the component’s investment cost as follows [27]:

$$\dot{Z}_k = \left(\frac{CRF \times \varphi}{N \times 3600}\right) Z_k \tag{32}$$

where \dot{Z}_k is the total investment cost rate for each component, φ is the system maintenance factor, N is the system operating hour in the year, and Z_k is the component’s investment cost.

The capital recovery factor is calculated as:

$$CRF = \frac{i_r(1 + i_r)^n}{(1 + i_r)^n - 1} \tag{33}$$

where i_r is an interest rate that compensates for investment in equipment and n is the system life.

Optimization method

There are different evolutionary optimization algorithms such as differential evolution algorithms (DE) [33, 34], harmony search algorithm (HS) [35, 36] and genetic algorithm (GA) [37]. The evolutionary algorithms are based on Darwinian evolution which are well-known and are employed to optimize complex engineering problems such as fluid dynamics optimization [38], metallurgical problems [39] and thermodynamic systems [40]. Genetic algorithms are global optimization methods that search for optimums through the imitation of the natural evolution of biological organisms [41]. The optimization was done by NSGA-II (non-dominated sorting genetic algorithm). NSGA-II algorithm optimize the function by keeping elites of each population. Elites are fine results of the previous populations [42]. Multi-objective optimization has been conducted to maximize COP and minimize the refrigeration cost rate using MATLAB genetic algorithm. Multi-objective optimization is used when there is a conflict between the objectives [43]. In refrigeration systems, by increasing COP, the cost rate increases which is a conflict. Indeed, there is a trade-off between COP and cost rate.

Table 7 Exergy and exergo-economic results for each stream

State	Fluid	$\dot{m}/\text{kg s}^{-1}$	$T/^\circ\text{C}$	P/kPa	$h/\text{kJ kg}^{-1}$	$s/\text{kJ kg}^{-1} \text{K}$	$e/\text{kJ kg}^{-1}$	$\dot{C}/\text{\$ h}^{-1}$
1	R744	0.0882	9.077	4400	423.8	1.791	200.1	3.584
2	R744	0.0882	68.18	9300	456.3	1.806	228.1	3.852
3	R744	0.0882	35	9300	295.4	1.303	217.1	3.668
4	R744	0.0882	25	9300	258.3	1.181	216.4	3.658
5	R744	0.1297	9.077	4400	356.1	1.551	203.9	5.393
6	R744	0.0675	9.077	4400	223.2	1.08	211.4	2.898
7	R744	0.0675	-35.06	1200	223.2	1.129	196.8	2.898
8	R744	0.0675	-35.06	1200	436.2	2.023	143.1	2.107
9	R744	0.0675	14	1200	484.7	2.209	136.3	2.235
10	R744	0.0675	130.5	4600	577.5	2.245	218.3	2.826
11	R744	0.0261	129.5	4400	577.5	2.253	216	1.090
12	water	0.2246	25	100	104.9	0.3672	0.00	0.000
13	water	0.1171	32	100	134.2	0.4642	0.3369	0.013
14	water	0.1171	61	100	255.4	0.8438	8.416	0.316
15	water	0.2246	40	100	167.6	0.5724	1.525	0.233
16	air	2.86	-25	100	248.1	6.678	3.63	2.898
17	air	2.86	-30	100	243.1	6.657	4.704	3.755

Results and discussion

Base cycle result

The results of the base cycle analysis are presented in Table 7 and 8. It was discovered that ejector outlet flow has the highest cost rate ($5.393 \text{ \$ h}^{-1}$). The refrigeration cost rate (C_7) is $2.898 \text{ \$ h}^{-1}$. The water mass flow rate of the gas cooler was calculated as 0.1171 kg s^{-1} . The low compressor discharge temperature is $130.5 \text{ }^\circ\text{C}$ which is the

Table 8 Exergy results for each component of the cycle

Component	η_k	δ_k	\dot{E}_r/kW	\dot{E}_p/kW	\dot{E}_D/kW
Gas cooler	0.971	0.006	0.9736	0.9457	0.02793
Internal heat exchanger	0.125	0.087	0.4616	0.0579	0.4037
Ejector	0.540	0.110	1.106	0.5968	0.5092
Intercooler	0.995	0.032	32.06	31.92	0.1463
Expansion valve 1	0.807	0.211	5.083	4.102	0.9809
Evaporator	0.847	0.119	3.627	3.074	0.5533
Low-pressure compressor	0.883	0.158	6.266	5.536	0.7308
High-pressure compressor	0.863	0.084	2.867	2.475	0.3917
Expansion valve 2	0.879	0.013	0.4979	0.4378	0.06004
Thermo-electric generator	0.116	0.180	0.9457	0.1093	0.8364

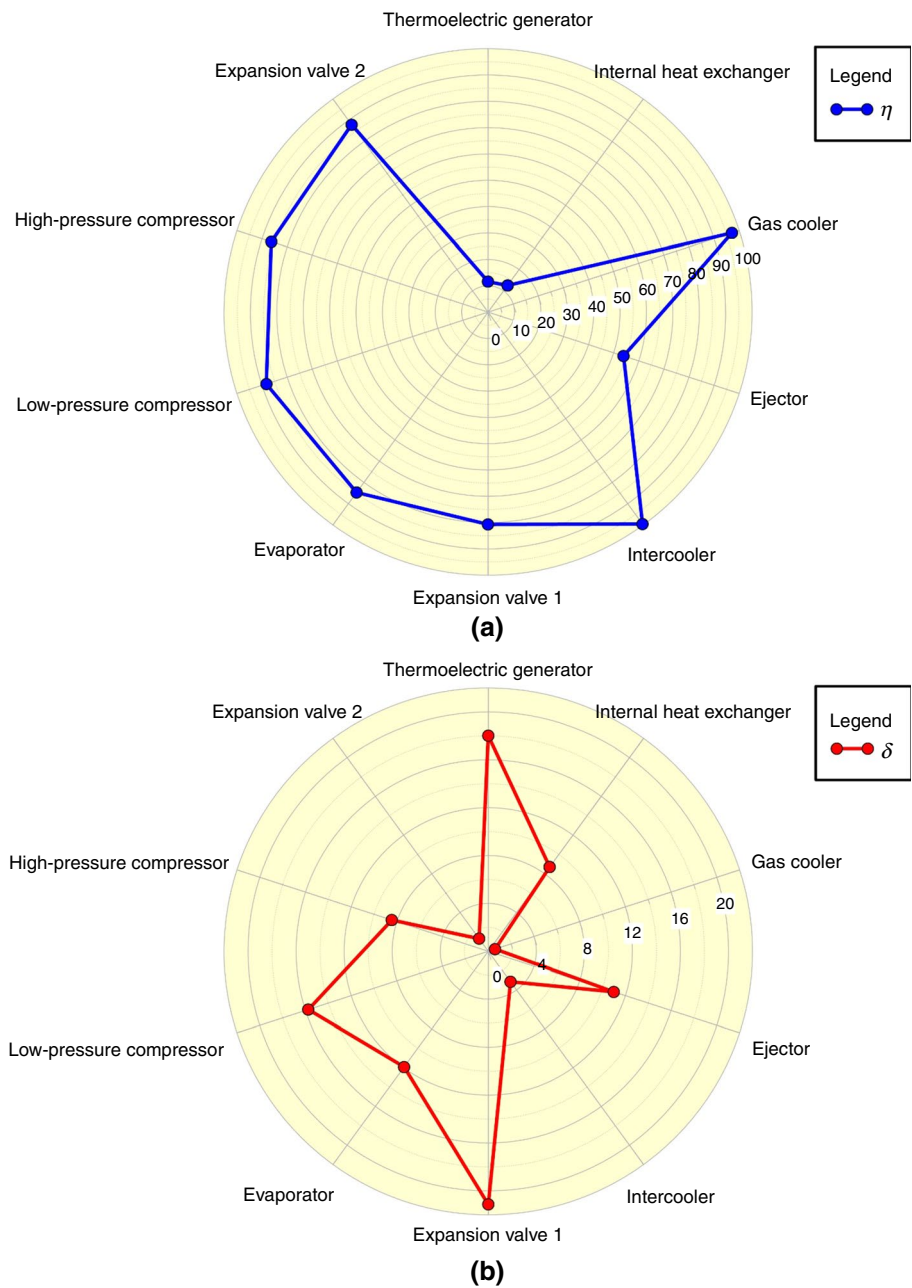
highest temperature in the refrigeration cycle. The COP of the base cycle is calculated as 1.593 which has increased by 27.24% in comparison to Ref. [20]. The ejector entrainment ratio was calculated as 0.47. The exergy efficiency and exergy destruction ratio of the cycle, are $\eta_{ex} = 0.3485$, $\delta_{ex} = 0.5081$

According to Table 8, expansion valve 1, thermo-electric generator, and low-pressure compressor have the highest exergy destruction rate as 0.9809 kW, 0.8364 kW, and 0.7308 kW respectively. The intercooler, gas cooler, and low-pressure compressor have the highest exergy efficiency which are 0.995, 0.971, and 0.883. Expansion valve 1, thermo-electric generator, and low-pressure compressor have the highest exergy destruction ratio as 0.211, 0.180, and 0.158 respectively; which are the high priorities for system improvement.

Parametric study results

To achieve a comprehensive view about performance of suggested system a parametric study has been conducted on the gas cooler, low-pressure compressor discharge pressure, and evaporator pressure for pressure ranges of 8800–20000 kPa, 4500–5500 kPa, and 800–1200 kPa, respectively (Fig. 5).

Fig. 5 **a** Efficiency and **b** exergy destruction ratio of each component



Gas cooler pressure effects

Figure 6a depicts the effect of gas cooler pressure on COP and C_7 . It was discovered by increasing gas cooler pressure, the COP of the cycle drops from 1.693 to 0.8289. Also, by increasing gas cooler pressure, the refrigeration cost rate (C_7) is approximately constant and it is roughly

2.864 \$ h⁻¹. According to Fig. 6b, it can be deduced that by increasing gas cooler pressure, total fuel exergy rate, exergy destruction ratio, and total exergy destruction rate, rise steadily but exergy efficiency of the cycle drops from 0.3686 to 0.1899. Figure 6c demonstrated how system components are affected by gas cooler pressure. As pressure rises, exergy destruction of the gas cooler, ejector, and

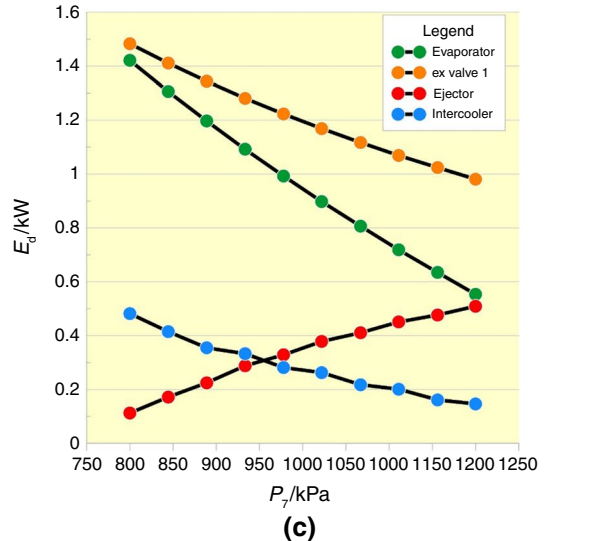
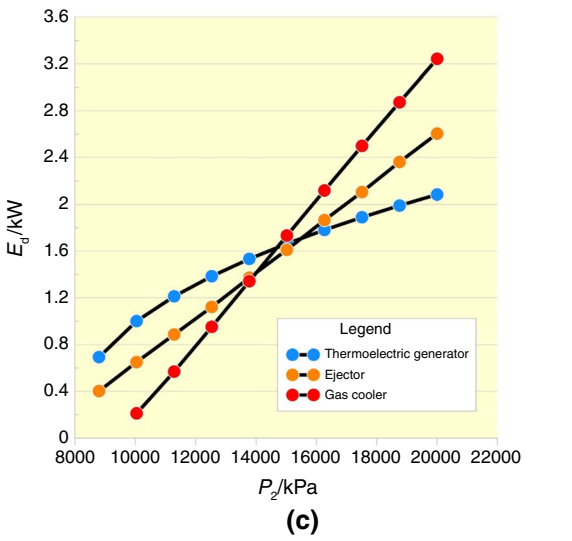
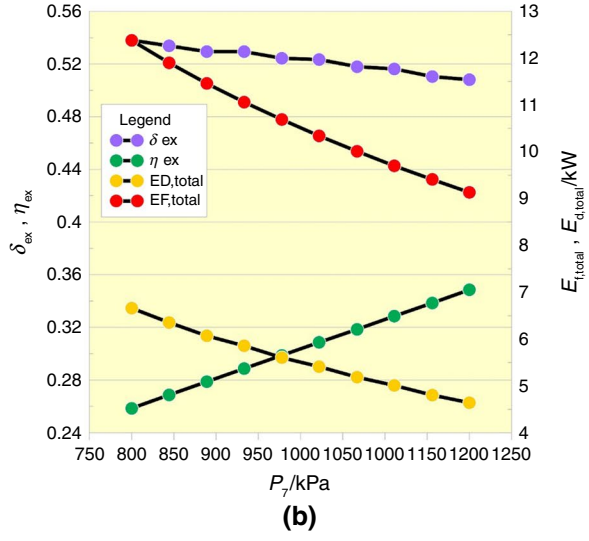
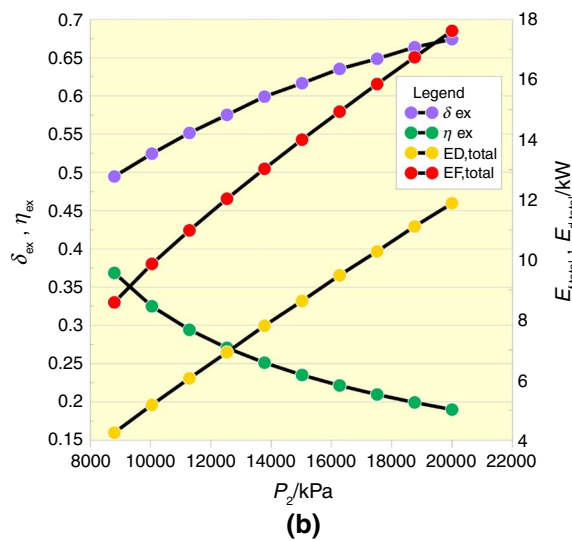
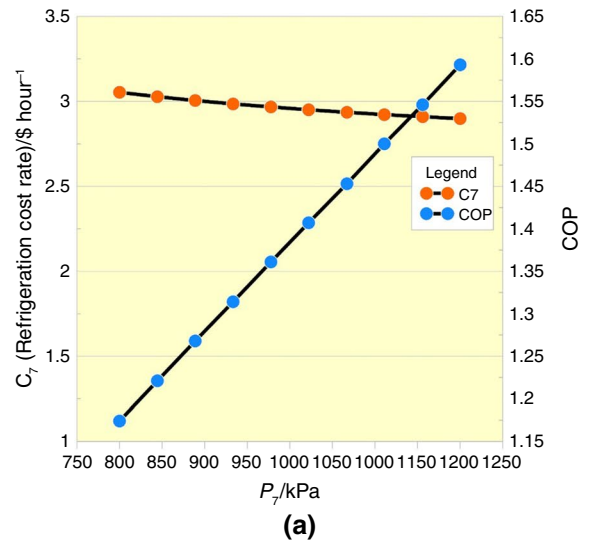
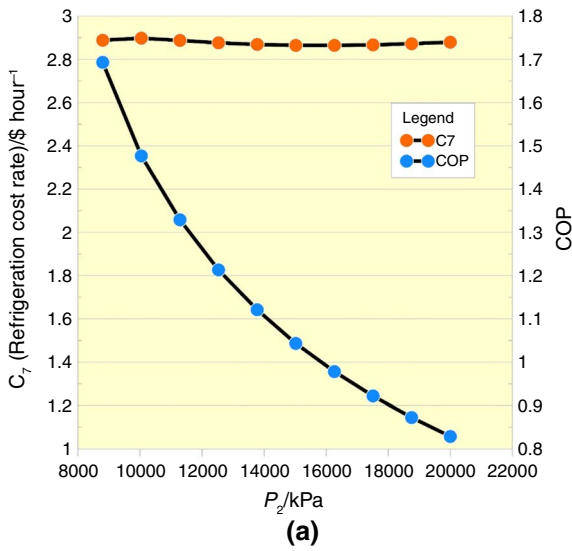


Fig. 6 a Effect of gas cooler pressure on refrigeration cost rate and COP b Effect of gas cooler pressure on cycle exergy destruction ratio, cycle efficiency, total exergy destruction, and total fuel exergy c Effect of gas cooler pressure on exergy destruction of components

Fig. 7 a Effect of evaporator pressure on refrigeration cost rate and COP. b Effect of evaporator pressure on cycle exergy destruction ratio, cycle efficiency, total exergy destruction, and total fuel exergy. c Effect of evaporator pressure on exergy destruction of components

Fig. 8 a Effect of discharge pressure of low-pressure compressor on refrigeration cost rate and COP. **b** Effect of discharge pressure of low-pressure compressor on cycle exergy destruction ratio, cycle efficiency, total exergy destruction, and total fuel exergy. **c** Effect of discharge pressure of low-pressure compressor on exergy destruction of components

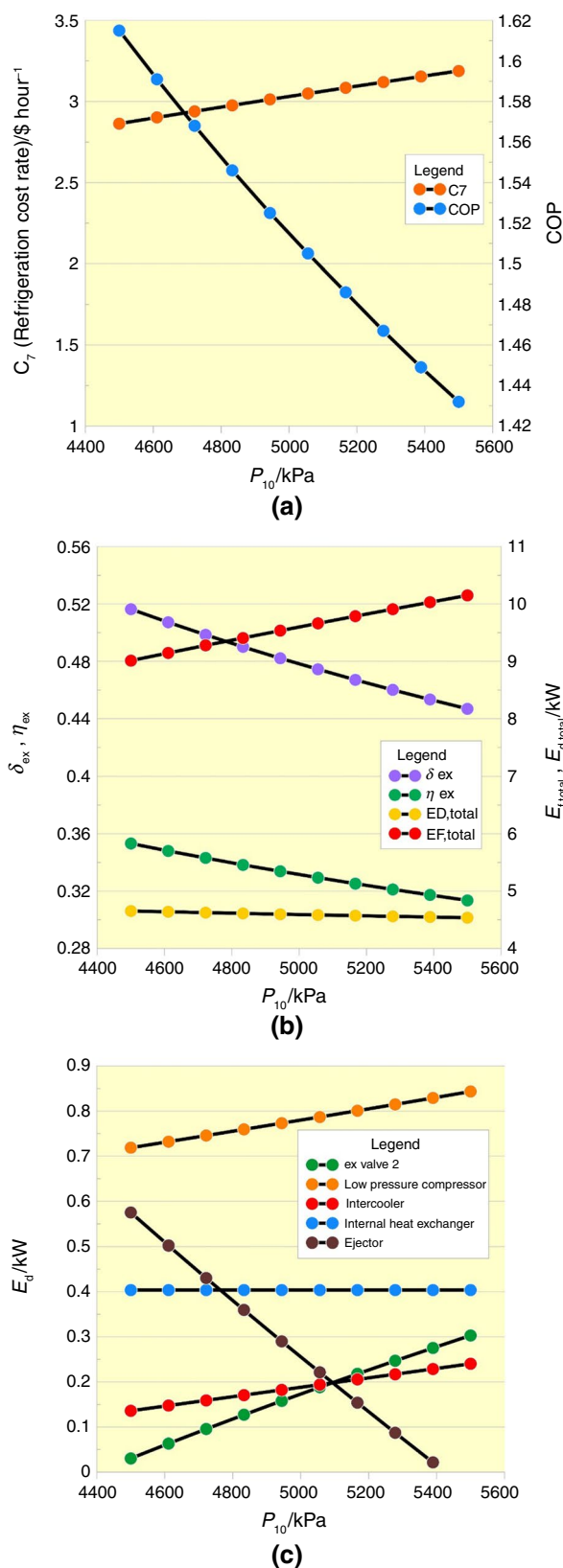
thermo-electric generator, increased. Gas cooler exergy destruction rate increased from 0.2113 kW to 3.243 kW which suggested reducing gas cooler pressure in order to reduce the exergy destruction rate of gas cooler to enhance system operation. The higher pressure of gas cooler could increase the input power of the compressor and also it could increase the outlet temperature of high-pressure compressor. Finally, it increased the exergy destruction of the compressor and gas cooler.

Evaporator pressure effects

Figure 7a demonstrated the effect of evaporator pressure on the COP and refrigeration cost rate. As depicted, by the rise of evaporator pressure, COP increased from 1.174 to 1.593 and the refrigeration cost rate decreased from 3.0528 \$ h⁻¹ to 2.898 \$ h⁻¹. Based on Fig. 7b by the rise of evaporator pressure, total fuel exergy rate, exergy destruction ratio, and total exergy destruction rate, decreased and exergy efficiency of the cycle increased by 34.82% (from 0.2585 to 0.3485). Figure 7c demonstrated the effect of evaporator pressure on exergy destruction of components. As evaporator pressure increased, the exergy destruction of the evaporator, expansion valve 1, and intercooler, decreased and exergy destruction of the ejector increased from 0.1122 kW to 0.5092 kW.

Discharge pressure of low-pressure compressor effects

According to Fig. 8a by increasing in discharge pressure of low-pressure compressor, COP decreased from 1.615 to 1.432 and the refrigeration cost rate increased from 2.863 \$ h⁻¹ to 3.189 \$ h⁻¹. Figure 8b depicts the effect of discharge pressure on total fuel exergy rate, exergy destruction ratio, total exergy destruction rate, and exergy efficiency. It can be seen that by increasing discharge pressure, total fuel exergy rate increased; and total exergy destruction rate, exergy destruction ratio and exergy efficiency of the overall system decreased. Figure 8c demonstrated the effect of discharge pressure on exergy destruction of components. As discharge pressure increased, exergy destruction rate of low-pressure compressor, expansion valve 2, and intercooler increased and exergy destruction rate of the ejector decreased due to higher secondary inlet exergy based on exergy balance for ejector.



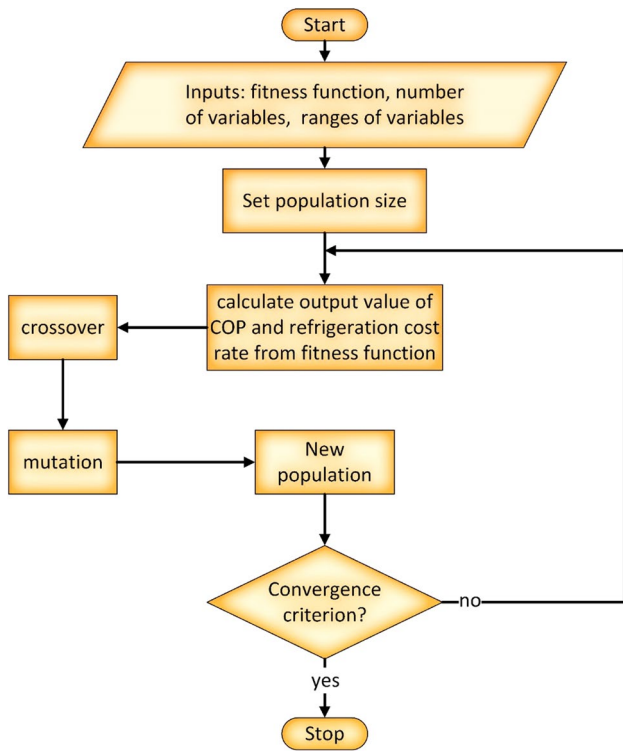


Fig. 9 Flowchart of multi-objective optimization

Table 9 Genetic algorithm options and parameter ranges for optimization

Property	Value
Population size	120
Maximum number of generations	18
Crossover fraction	0.8
Mutation fraction	0.2
Gas cooler pressure	8800–20000 kPa
Evaporator pressure	800–1200 kPa
Low-pressure compressor discharge pressure	4500- 5500 kPa

Multi-objective optimization results

As depicted in Fig. 9 firstly, the fitness function, number of variables, and the range of each variable was determined. Then the size of population was set. By using fitness function, the value of each individual was calculated. The new population was generated considering crossover and mutation fractions based on Table 9. The convergence criterion was the maximum number of generations. It was 15 for this process. Figure 10 is the Pareto frontier of optimization. Table 10 is the list of parameters for the corresponding points in Pareto frontier. According to the optimization

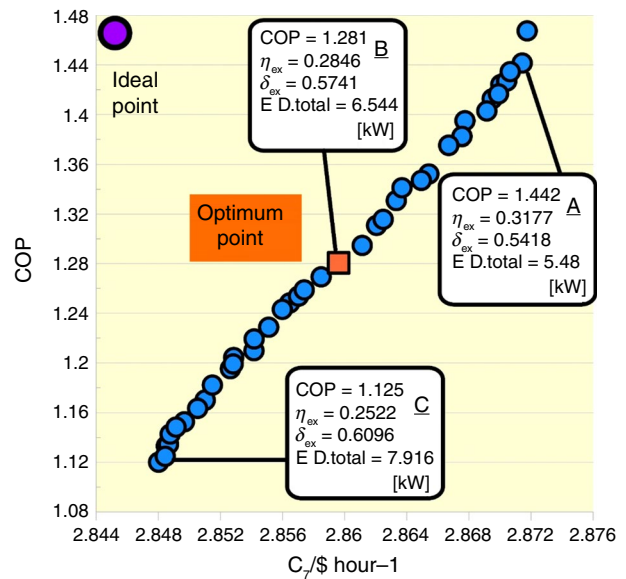


Fig. 10 Multi-objective optimization result (Pareto frontier)

Table 10 Multi-objective optimization results

point	Decision variables $\dot{C}_7 (\$ h^{-1})$	Decision variables			
		COP	P_2 / kPa	P_7 / kPa	P_{10} / kPa
A	2.871	1.442	10,402.41	1197.82	4521.45
B	2.859	1.281	11,869.52	1197.44	4518.70
C	2.848	1.125	13,814.26	1197.00	4518.05

outputs, the optimum design point, could provide the COP of 1.281. The exergy efficiency and the exergy destruction ratio of the optimum design point are 0.284 and 0.574, respectively and the exergy destruction rate of the optimum point is 6.544 kW.

Conclusions

A study on ejector two-stage trans-critical CO₂ refrigeration cycle which is equipped with a thermo-electric generator was conducted. The cycle modeled using Engineering Equation Solver (EES) and the optimization was done using MATLAB multi-objective optimization utility. One of the main purposes of this study was to evaluate the effect of thermo-electric generator in the cycle. Thermo-electric generator, recovers energy from waste heat of gas cooler thus it could reduce the inlet work of compressors and consequently increase the COP. The refrigeration system was assessed from energy, exergy, and exergo-economic viewpoints.

The China business electricity price [32] was used for the value of compressors specific exergy cost (c_w). According to exergy analysis result, low-pressure expansion valve, low-pressure compressor, and evaporator have the highest exergy destruction rate. The coefficient of performance was obtained as 1.593. The ejector entrainment ratio was 0.47. The exergy efficiency and exergy destruction ratio of the system, were 0.3485 and 0.5081, respectively. The results of the simulation show expansion valve 1, thermo-electric generator, and low-pressure compressor have the highest exergy destruction rate as 0.9809 kW, 0.8364 kW, and 0.7308 kW, respectively. The important results were obtained are:

- δ_{ex} Increases by increasing the gas cooler pressure.
- δ_{ex} Decreases by increasing the evaporator pressure.
- According to optimization outputs, the optimum pressures for low-pressure compressor outlet and evaporator are about 4518.70 kPa and 1197.44 kPa, respectively.
- Expansion valve 2 acts as a control valve and it transfers the excess part of the low-pressure compressor outflow to the intercooler.
- The optimum COP of the system was 1.281.
- The total exergy destruction rate varies from 5.48 kW to 7.916 kW based on optimization results.
- The exergy efficiency and the exergy destruction ratio of the optimum design point are 0.284 and 0.574.

Further work is needed to assess the impact of different refrigerant on system performance. Another important analysis could be exergo-environmental analysis which could be combined with exergy and exergo-economic analysis to improve the environmental impact of the system. Furthermore, a renewable energy source could be used to supply the cycle. Solar photovoltaic panel could be employed to produce power and supply the compressors.

Acknowledgements Authors would like to acknowledge the financial support of Kermanshah University of Technology for this research under grant number S/T/P/1430.

References

1. Mosaffa AH, Farshi LG, Infante Ferreira CA, Rosen MA. Exergoeconomic and environmental analyses of CO₂/NH₃ cascade refrigeration systems equipped with different types of flash tank intercoolers. *Energy Convers Manag.* 2016;117:442–53. <https://doi.org/10.1016/j.enconman.2016.03.053>.
2. Haq MdZ, Ayon MdSR, Nouman MdWB, Bihani R. Thermodynamic analysis and optimisation of a novel transcritical CO₂ cycle. *Energy Convers Manag.* 2022;273: 116407. <https://doi.org/10.1016/j.enconman.2022.116407>.
3. Yu B, Yang J, Wang D, Shi J, Chen J. An updated review of recent advances on modified technologies in transcritical CO₂ refrigeration cycle. *Energy.* 2019;189: 116147. <https://doi.org/10.1016/j.energy.2019.116147>.
4. Dai B, Liu S, Zhu K, Sun Z, Ma Y. Thermodynamic performance evaluation of transcritical carbon dioxide refrigeration cycle integrated with thermoelectric subcooler and expander. *Energy.* 2017;122:787–800. <https://doi.org/10.1016/j.energy.2017.01.029>.
5. Qyyum MA, Naquash A, Sial NR, Lee M. CO₂ precooled dual phase expander refrigeration cycles for offshore and small-scale LNG production: energy, exergy, and economic evaluation. *Energy.* 2023;262: 125378. <https://doi.org/10.1016/j.energy.2022.125378>.
6. Mansour A, Oberti R, Nesreddine H, Poncet S. Thermodynamic analysis of a transcritical CO₂ heat pump integrating a vortex tube. *Appl Therm Eng.* 2023;224: 120076. <https://doi.org/10.1016/j.applthermaleng.2023.120076>.
7. Huang C, Li Z, Ye Z, Wang R. Thermodynamic study of carbon dioxide transcritical refrigeration cycle with dedicated subcooling and cascade recooling. *Int J Refrig.* 2022;137:80–90. <https://doi.org/10.1016/j.ijrefrig.2022.02.004>.
8. Dai B, Liu S, Sun Z, Ma Y. Thermodynamic performance analysis of CO₂ transcritical refrigeration cycle assisted with mechanical subcooling. *Energy Procedia.* 2017;105:2033–8. <https://doi.org/10.1016/j.egypro.2017.03.579>.
9. Chen X, Yang Q, Chi W, Zhao Y, Liu G, Li L. Energy and exergy analysis of NH₃/CO₂ cascade refrigeration system with subcooling in the low-temperature cycle based on an auxiliary loop of NH₃ refrigerants. *Energy Rep.* 2022;8:1757–67. <https://doi.org/10.1016/j.egypr.2022.01.004>.
10. Aghazadeh Dokandari D, Setayesh Hagh A, Mahmoudi SMS. Thermodynamic investigation and optimization of novel ejector-expansion CO₂/NH₃ cascade refrigeration cycles (novel CO₂/NH₃ cycle). *Int J Refrig.* 2014;46:26–36. <https://doi.org/10.1016/j.ijrefrig.2014.07.012>.
11. Braimakis K. Solar ejector cooling systems: a review. *Renew Energy.* 2021;164:566–602. <https://doi.org/10.1016/j.renene.2020.09.079>.
12. Liu J, Liu Y, Yu J. Performance analysis of a modified dual-ejector and dual-evaporator transcritical CO₂ refrigeration cycle for supermarket application. *Int J Refrig.* 2021;131:109–18. <https://doi.org/10.1016/j.ijrefrig.2021.06.010>.
13. Eskandari Manjili F, Cheraghi M. Performance of a new two-stage transcritical CO₂ refrigeration cycle with two ejectors. *Appl Therm Eng.* 2019;156:402–9. <https://doi.org/10.1016/j.applthermaleng.2019.03.083>.
14. Lee JS, Kim MS, Kim MS. Experimental study on the improvement of CO₂ air conditioning system performance using an ejector. *Int J Refrig.* 2011;34(7):1614–25. <https://doi.org/10.1016/j.ijrefrig.2010.07.025>.
15. Liu J, Zhou L, Lyu N, Lin Z, Zhang S, Zhang X. Analysis of a modified transcritical CO₂ two-stage ejector-compression cycle for domestic hot water production. *Energy Convers Manag.* 2022;269: 116094. <https://doi.org/10.1016/j.enconman.2022.116094>.
16. Wang Y, Yin Y, Cao F. Comprehensive evaluation of the transcritical CO₂ ejector-expansion heat pump water heater. *Int J Refrig.* 2023;145:276–89. <https://doi.org/10.1016/j.ijrefrig.2022.09.008>.
17. Casi Á, Aranguren P, Araiz M, Sanchez D, Cabello R, Astrain D. Performance assessment of an experimental CO₂ transcritical refrigeration plant working with a thermoelectric subcooler in combination with an internal heat exchanger. *Energy Convers Manag.* 2022;268: 115963. <https://doi.org/10.1016/j.enconman.2022.115963>.
18. Santini F, Bianchi G, Battista DD, Villante C, Orlandi M. Experimental investigations on a transcritical CO₂ refrigeration plant and theoretical comparison with an ejector-based one. *Energy Procedia.* 2019;161:309–16. <https://doi.org/10.1016/j.egypro.2019.02.097>.

19. Aranguren P, Sánchez D, Casi A, Cabello R, Astrain D. Experimental assessment of a thermoelectric subcooler included in a transcritical CO₂ refrigeration plant. *Appl Therm Eng.* 2021;190: 116826. <https://doi.org/10.1016/j.applthermaleng.2021.116826>.
20. Yang D, Jie Z, Zhang Q, Li Y, Xie J. Evaluation of the ejector two-stage compression refrigeration cycle with work performance from energy, conventional exergy and advanced exergy perspectives. *Energy Rep.* 2022;8:12944–57. <https://doi.org/10.1016/j.egy.2022.09.108>.
21. Liu X, Fu R, Wang Z, Lin L, Sun Z, Li X. Thermodynamic analysis of transcritical CO₂ refrigeration cycle integrated with thermoelectric subcooler and ejector. *Energy Convers Manag.* 2019;188:354–65. <https://doi.org/10.1016/j.enconman.2019.02.088>.
22. Chen G, Volovyk O, Zhu D, Ierin V, Shestopalov K. Theoretical analysis and optimization of a hybrid CO₂ transcritical mechanical compression–ejector cooling cycle. *Int J Refrig.* 2017;74:86–94. <https://doi.org/10.1016/j.ijrefrig.2016.10.002>.
23. Wang X, Yu J, Zhou M, Lv X. Comparative studies of ejector-expansion vapor compression refrigeration cycles for applications in domestic refrigerator-freezers. *Energy.* 2014;70:635–42. <https://doi.org/10.1016/j.energy.2014.04.076>.
24. Liu Q, He Z, Liu Y, He Y. Thermodynamic and parametric analyses of a thermoelectric generator in a liquid air energy storage system. *Energy Convers Manag.* 2021;237: 114117. <https://doi.org/10.1016/j.enconman.2021.114117>.
25. Tian Z, Chen X, Zhang Y, Gao W, Chen W, Peng H. Energy, conventional exergy and advanced exergy analysis of cryogenic recuperative organic rankine cycle. *Energy.* 2023;268: 126648. <https://doi.org/10.1016/j.energy.2023.126648>.
26. Zheng L, Hu Y, Mi C, Deng J. Advanced exergy analysis of a CO₂ two-phase ejector. *Appl Therm Eng.* 2022;209: 118247. <https://doi.org/10.1016/j.applthermaleng.2022.118247>.
27. Abdolalipouradl M, Mohammadkhani F, Khalilarya S, Yari M. Thermodynamic and exergoeconomic analysis of two novel tri-generation cycles for power, hydrogen and freshwater production from geothermal energy. *Energy Convers Manag.* 2020;226: 113544. <https://doi.org/10.1016/j.enconman.2020.113544>.
28. Liu J, Liu Y, Yan G, Yu J. Theoretical study on a modified single-stage autocascade refrigeration cycle with auxiliary phase separator. *Int J Refrig.* 2021;122:181–91. <https://doi.org/10.1016/j.ijrefrig.2020.11.009>.
29. Al-Rashed AAAA, Afrand M. Multi-criteria exergoeconomic optimization for a combined gas turbine-supercritical CO₂ plant with compressor intake cooling fueled by biogas from anaerobic digestion. *Energy.* 2021;223: 119997. <https://doi.org/10.1016/j.energy.2021.119997>.
30. Baniasad Askari I, Shahsavari A. The exergo-economic analysis of two novel combined ejector heat pump/humidification-dehumidification desalination systems. *Sustain Energy Technol Assess.* 2022;53:102561. <https://doi.org/10.1016/j.seta.2022.102561>.
31. Khanmohammadi S, Musharavati F, Kizilkan O, Duc Nguyen D. Proposal of a new parabolic solar collector assisted power-refrigeration system integrated with thermoelectric generator using 3E analyses: energy, exergy, and exergo-economic. *Energy Convers Manag.* 2020;220:113055. <https://doi.org/10.1016/j.enconman.2020.113055>.
32. “Gasoline and diesel prices by country,” GlobalPetrolPrices.com. Accessed: Aug. 06, 2023. [Online]. Available: <https://www.globalpetrolprices.com/>
33. Jahromi FS, Beheshti M, Rajabi RF. Comparison between differential evolution algorithms and response surface methodology in ethylene plant optimization based on an extended combined energy - exergy analysis. *Energy.* 2018;164:1114–34. <https://doi.org/10.1016/j.energy.2018.09.059>.
34. Qudah A, Almerbati A, Mokheimer EMA. Novel approach for optimizing wind-PV hybrid system for RO desalination using differential evolution algorithm. *Energy Convers Manag.* 2024;300: 117949. <https://doi.org/10.1016/j.enconman.2023.117949>.
35. Karmakar R, Chatterjee S, Datta D, Chakraborty D. Application of harmony search algorithm in optimizing autoregressive integrated moving average: a study on a data set of Coronavirus Disease 2019. *Syst Soft Comput.* 2024;6: 200067. <https://doi.org/10.1016/j.sasc.2023.200067>.
36. Lee GH, Sadollah A, Park SH, Geem ZW. HS-Solver: Spreadsheet based harmony search algorithm solver for various optimization problems. *SoftwareX.* 2022;20: 101262. <https://doi.org/10.1016/j.softx.2022.101262>.
37. Cheng H, et al. Economic, environmental, exergy (3E) analysis and multi-objective genetic algorithm optimization of efficient and energy-saving separation of diethoxymethane/toluene/ethanol by extractive distillation with mixed extractants. *Energy.* 2023;284: 129262. <https://doi.org/10.1016/j.energy.2023.129262>.
38. Kaseb Z, Rahbar M. Towards CFD-based optimization of urban wind conditions: comparison of genetic algorithm, particle swarm optimization, and a hybrid algorithm. *Sustain Cities Soc.* 2022;77: 103565. <https://doi.org/10.1016/j.scs.2021.103565>.
39. Vuolio T, Visuri V-V, Sorsa A, Ollila S, Fabritius T. Application of a genetic algorithm based model selection algorithm for identification of carbide-based hot metal desulfurization. *Appl Soft Comput.* 2020;92: 106330. <https://doi.org/10.1016/j.asoc.2020.106330>.
40. Zhang L, et al. Integrated optimization for utilizing iron and steel industry’s waste heat with urban heating based on exergy analysis. *Energy Convers Manag.* 2023;295: 117593. <https://doi.org/10.1016/j.enconman.2023.117593>.
41. Erodoutou P, Voutsas E, Sarimveis H. A genetic algorithm approach for parameter estimation in vapour-liquid thermodynamic modelling problems. *Comput Chem Eng.* 2020;134: 106684. <https://doi.org/10.1016/j.compchemeng.2019.106684>.
42. Deb K, Goel T. Controlled Elitist Non-dominated Sorting Genetic Algorithms for Better Convergence. In: Zitzler E, Thiele L, Deb K, Coello Coello CA, Corne D, editors. In: *Evolutionary Multi-Criterion Optimization*. Berlin, Heidelberg: Springer, Berlin Heidelberg; 2001.
43. Pan M, et al. Thermodynamic, exergoeconomic and multi-objective optimization analysis of new ORC and heat pump system for waste heat recovery in waste-to-energy combined heat and power plant. *Energy Convers Manag.* 2020;222: 113200. <https://doi.org/10.1016/j.enconman.2020.113200>.

Publisher's Note Springer Nature remains neutral with regard to jurisdictional claims in published maps and institutional affiliations.

Springer Nature or its licensor (e.g. a society or other partner) holds exclusive rights to this article under a publishing agreement with the author(s) or other rightsholder(s); author self-archiving of the accepted manuscript version of this article is solely governed by the terms of such publishing agreement and applicable law.